Position-dependent and millimetre-range photodetection in phototransistors with micrometre-scale graphene on SiC

Biddut K. Sarker[1,2†], Edward Cazalas[3†], Ting-Fung Chung[1,2†], Isaac Childres[1,2], Igor Jovanovic[3,4] and Yong P. Chen[1,2,5,6★]

The extraordinary optical and electronic properties of graphene make it a promising component of high-performance photodetectors. However, in typical graphene-based photodetectors demonstrated to date, the photoresponse only comes from specific locations near graphene over an area much smaller than the device size. For many optoelectronic device applications, it is desirable to obtain the photoresponse and positional sensitivity over a much larger area. Here, we report the spatial dependence of the photoresponse in backgated graphene field-effect transistors (GFET) on silicon carbide (SiC) substrates by scanning a focused laser beam across the GFET. The GFET shows a nonlocal photoresponse even when the SiC substrate is illuminated at distances greater than 500 μm from the graphene. The photoresponsivity and photocurrent can be varied by more than one order of magnitude depending on the illumination position. Our observations are explained with a numerical model based on charge transport of photoexcited carriers in the substrate.

Graphene-based photodetectors have attracted significant attention recently due to their ultrafast and broadband response, features that are important for next-generation optoelectronic applications such as imaging, high-speed communication, spectroscopy and displays[1–23]. One of the major challenges hindering applications of graphene-based photodetectors is their small effective photosensitive area. The graphene-based photodetectors demonstrated so far only show a local photoresponse, when the light is illuminated on specific device areas on the graphene or its boundary, such as at the metal–graphene interface on the contacts[3,8,9], at the p–n junction in the graphene[19,23], at the interface between single-layer and bilayer graphene[20], or at the hybrid channel where graphene is in contact with other photoactive nanomaterials (such as semiconductor quantum dots or two-dimensional materials)[13,14]. This is because the photoresponse in these photodetectors requires light absorption in the channel that includes or is in direct contact with graphene. The photoresponsivity quickly falls off to zero for illumination outside those specific locations within the device active areas. In many sensing applications, precise illumination onto specific device locations is not always feasible, resulting in no photoresponse or a response derived from only a small fraction of the illuminating power. To overcome those limitations, it is important to develop graphene photodetectors that can be operated without precise illumination on the graphene or contacts, and to examine their position-sensitive photoresponse characteristics.

In this Article, we investigate, for the first time, the position-sensitive, nonlocal and large-area photoresponse of photo-actuated graphene field-effect transistors (GFETs) on undoped silicon carbide (SiC) substrates by illuminating them at various positions using a focused laser beam. We show that the unique and simple combination of small-area graphene and large-area SiC substrate provides both position sensitivity and large-area photodetection. We demonstrate that a photoresponse can be achieved for laser illumination not only on the graphene channel, but also on the bare SiC substrate a few hundred micrometres away from the graphene (for example, more than 500 μm away for a low incident laser power of 5 μW). For light illumination within ~100 μm of the graphene, the device can show a strong photocurrent signal with a room-temperature photoresponsivity exceeding ~10 A W^{-1} (reaching ~18 A W^{-1} when the illumination is on the graphene). The photoresponse characteristics of our device (for example, photocurrent, photoresponsivity and response time) can be varied by over one order of magnitude by varying the distance of laser illumination from the graphene. We qualitatively explain the position-sensitive photoresponse based on the dependence of the electric field in the SiC substrate near the graphene on the position of illumination, because the graphene conductivity is determined by the change in this local electric field. We also develop a model that quantitatively explains the experimentally observed position-dependent photoresponse by considering the transport of photo-generated charge carriers to near the graphene.

A schematic of a GFET on an undoped SiC substrate is shown in Fig. 1a. The GFETs are fabricated by transferring mechanically exfoliated single-layer graphene onto an undoped SiC substrate, followed by electron-beam lithography and metal deposition of the contacts (see Methods). The device electrical response is measured while a focused laser beam (spot size ~0.6 μm) with a wavelength of 532 nm illuminates various locations on the device (Fig. 1b,c). Although the excitation energy of the laser (2.3 eV) is slightly below the nominal bandgap of SiC (ranging from 2.4 to 3.3 eV)[24], SiC can absorb 532 nm incident light and generate

[1]Department of Physics and Astronomy, Purdue University, West Lafayette, Indiana 47907, USA. [2]Birck Nanotechnology Center, Purdue University, West Lafayette, Indiana 47907, USA. [3]Department of Mechanical and Nuclear Engineering, The Pennsylvania State University, University Park, Pennsylvania 16802, USA. [4]Department of Nuclear Engineering and Radiological Sciences, University of Michigan, Ann Arbor, Michigan 48109, USA. [5]School of Electrical and Computer Engineering, Purdue University, West Lafayette, Indiana 47907, USA. [6]Purdue Quantum Center, Purdue University, West Lafayette, Indiana 47907, USA. [†]These authors contributed equally to this work. *e-mail: yongchen@purdue.edu
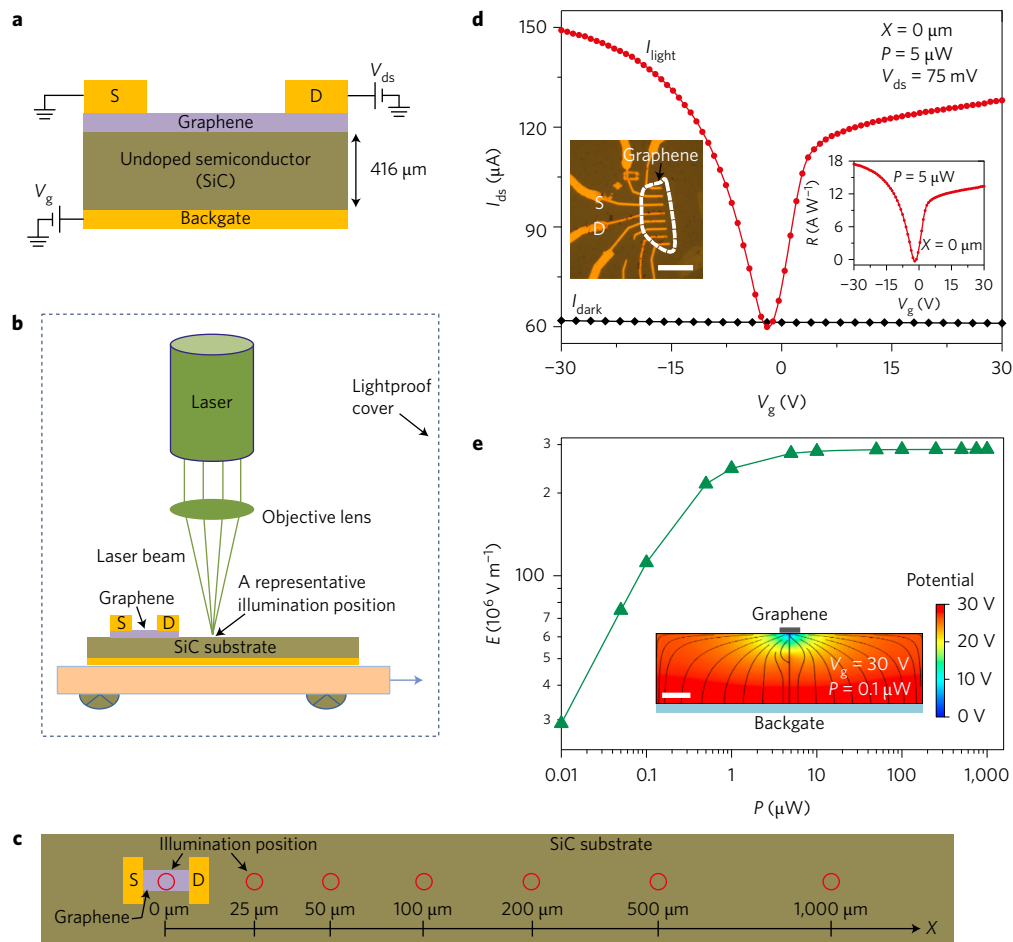
Figure 1 | Graphene phototransistor and gate voltage-tunable photocurrent. a, Schematic of a graphene field-effect transistor (GFET) together with electrical connections used to characterize the device. **b**, Schematic of the position-dependent photoresponse measurement set-up. **c**, The position of laser illumination (red circles) on the device (both on graphene and on the SiC substrate away from the graphene), where X denotes the distance of the illumination position from the centre of the graphene channel. **d**, Dependence of drain–source current on backgate voltage (I_{ds} – V_g) of a GFET at a drain–source voltage (V_{ds}) of 75 mV, without and with laser (λ = 532 nm) illumination on the graphene (X = 0 µm). The incident laser power on the device is 5 µW and the beam spot size is ~0.6 µm. All measurements were conducted under ambient conditions. In the absence of light ('dark'), due to the relatively large thickness ($d \approx 416$ µm) of the SiC substrate, the electric field experienced by the graphene is relatively small, giving rise to a weak field effect. Under laser illumination, photoexcited charge carriers are generated in the SiC, which increases the average conductivity of the SiC, resulting in an increase in the electric field. The photo-actuated change in the electric field is indirectly measured by the change in the graphene conductivity via the field effect, allowing us to detect light interacting with SiC. Inset (right): photoresponsivity R as a function of V_g for illumination position X = 0 µm. The maximum photoresponsivity of our device is ~18 A W^{-1}. Inset (left): optical image of a fabricated GFET (scale bar, 4 µm). **e**, Plot of electric field E (calculated with COMSOL Multiphysics) directly under the graphene of a GFET as a function of P at V_g = 30 V (for laser illumination on graphene, X = 0 µm). This shows that the electric field can be enhanced significantly by light illumination. Inset: representative simulation of electrical potential and electric field lines in the substrate (scale bar, 100 µm) for P = 0.1 µW. The electric field directs the photogenerated carriers toward the location under the graphene. With increasing P, E increases and the change in E is detected by the change in the conductivity of graphene, enabling the detection of light incident on the device.

photoexcited carriers due to in-gap impurity levels[24,25]. The nonlocal, position-dependent photoresponse data presented in the following sections are measured for one representative device with an illumination laser wavelength of 532 nm. A qualitatively similar photoresponse has also been reproduced in other devices and using other illumination laser wavelengths (Supplementary Section 4).

Field effect and photoresponse

We first characterized the photoresponse by focusing the laser beam on the graphene (X = 0 µm, where X denotes the distance of the illumination position from the centre of the graphene channel). Figure 1d presents the transfer curves, that is, drain–source current as a function of backgate voltage (I_{ds} – V_g), of the representative device measured both in the dark and under illumination with a laser power P of 5 µW. The dependence of the dark current I_{dark} on V_g is very small, indicating a weak field effect under dark conditions.

Due to the large thickness ($d \approx 416$ µm) of the undoped and insulating SiC substrate, a small electric field is experienced by the graphene without illumination (Fig. 1d), leading to a weak field effect. The current under illumination (I_{light}) is sharply increased for both high positive and negative V_g, with a minimum current at V_g = −2 V (defined as the Dirac point voltage, V_{Dirac}, the backgate voltage at the charge neutrality point), indicating that the charge carrier modulation and field effect in graphene are significantly enhanced upon light illumination. The device shows a photoresponsivity ($R = I_{photo}/P$, where photocurrent $I_{photo} = I_{light} - I_{dark}$) as high as 18 A W^{-1} at V_g = −30 V (Fig. 1d, right inset, and Supplementary Section 13). The photodetection gain of our device is ~42. This enhancement of charge carrier modulation and field effect in graphene is attributed to the generation of photo-excited charge carriers in SiC upon light illumination, which increases the conductivity of SiC in the regions where the
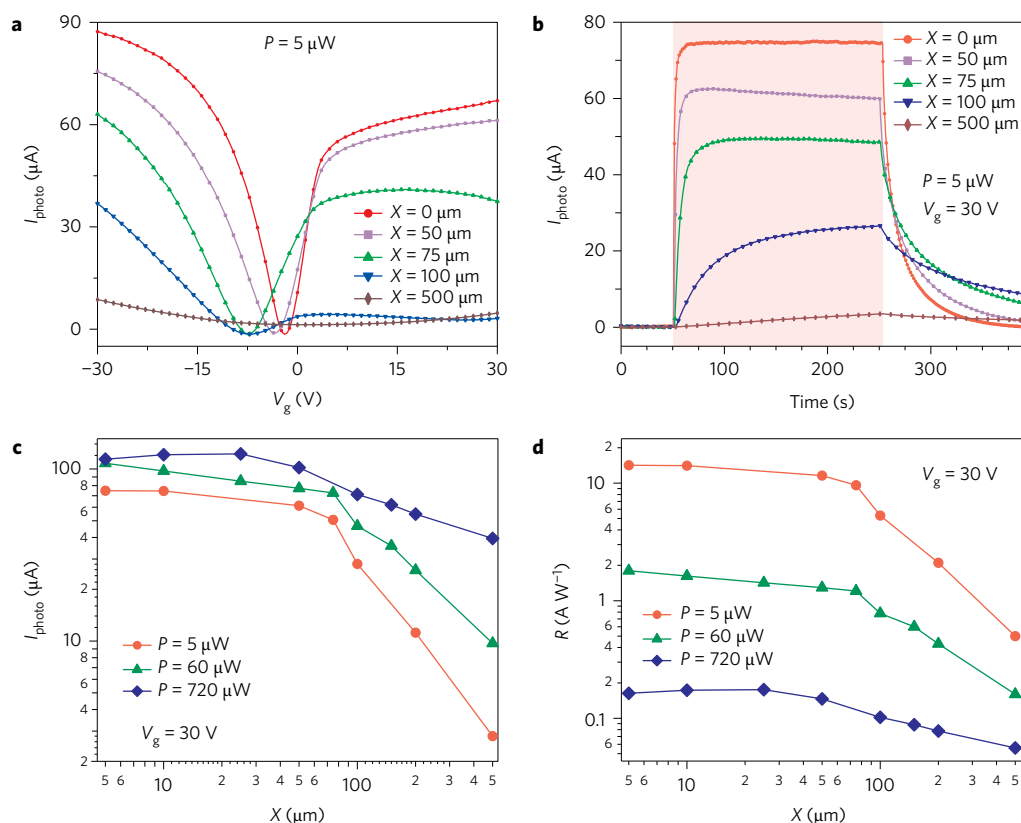
Figure 2 | Position-dependent photocurrent field effect and photocurrent dynamics. a, Photocurrent ($I_{photo} = I_{light} - I_{dark}$) as a function of gate voltage V_g of the GFET measured by laser illumination ($P = 5$ μW incident on the device) for a few representative positions ($X = 0$, 50, 75, 100 and 500 μm) on the device. For $X = 0$ μm, a strong gate-tunable photocurrent with a minimum at $V_g \approx -2$ V, which we define as the Dirac point voltage (V_{Dirac}), is observed. The shapes of I_{photo}–V_g curves change and V_{Dirac} shifts with increasing X. For larger values of X, the I_{photo}–V_g curves become nearly independent of V_g and no Dirac point is observed. **b**, Time-dependent photocurrent for a few illumination positions while the laser is switched on and off. Photocurrent data were measured with $P = 5$ μW, $V_{ds} = 75$ mV and $V_g = 30$ V. The shaded area indicates the time intervals during which the laser is on. The photocurrent response strongly depends on the illumination position and is observed for a laser illumination position up to ~500 μm away from the graphene. **c,d**, Log–log plots of the dependence of photocurrent (**c**) and photoresponsivity R (**d**) on the illumination position, measured at different incident laser powers. The device exhibits a notable photoresponsivity (~500 mA W^{-1} at $P = 5$ μW and ~60 mA W^{-1} at $P = 720$ μW), even for the laser illumination position 500 μm away from the graphene. All data were measured in these figures with $V_{ds} = 75$ mV and $V_g = 30$ V.

light is absorbed and leads to an increase in the electric field at the graphene in the presence of the backgate voltage. The change in the electric field changes the carrier density in the graphene and thus the conductivity of graphene[26]. In this way, the change in graphene conductivity is used to detect the light interacting with SiC via the field effect. This field-effect-based photodetection mechanism is also consistent with the observation of near-zero photocurrent at $V_g \approx 0$ V, when there is no electric field (and thus no field effect) to modulate the graphene conductivity. The small offset of the zero crossing point of the photocurrent away from $V_g = 0$ V (Fig. 1d) may be related to gate hysteresis and trapped charges in the SiC[27].

To further confirm the photodetection mechanism as well as to test the importance of the graphene in our devices, we also fabricated and measured two different control devices without graphene: (1) a SiC device (where the source and drain contacts are directly deposited on the SiC without graphene) and (2) a dummy device (where gold is used in the channel instead of graphene). These control devices showed a negligible photoresponse (Supplementary Section 2). In addition, the gate leakage current of the GFETs was small (below 1 nA, even when the device was illuminated with photons with energy close to the SiC bandgap) and did not change appreciably upon illumination (Supplementary Sections 3 and 4). This confirms that the SiC substrate in our device does not become sufficiently conductive to form a shorted electrical

connection between the backgate and the graphene, suggesting a significant fraction of the substrate remains insulating. The insulating behaviour probably originates from the inhomogeneous distribution of the photoexcited carriers or the existence of a native oxide layer, which often forms naturally on the SiC surface[28,29]. These control measurements, together with our observation of the photoresponse for light illumination away from the graphene or contact, confirm that the photoresponse of our GFETs is not derived from the Schottky junction between the SiC and metal contact or graphene, from the field effect in SiC, or from charge collection in the SiC; rather, it results from the charge carrier modulation and field effect in graphene due to photocarrier generation in SiC. When the GFETs are illuminated at a lower excitation energy (0.8 eV, which is much lower than the SiC bandgap), the device shows a much weaker field effect and negligible photoresponse (Supplementary Section 4), again confirming that photocarrier generation in SiC is responsible for the strong field effect and large photoresponse in our device.

To develop a better understanding of this photo-induced field-effect photodetection mechanism, we modelled the GFETs and conducted finite-element method (FEM) simulations (Supplementary Sections 1 and 9)[26]. A representative simulation of the electric potential and field lines in SiC under graphene is presented in the inset of Fig. 1e, showing a sharp increase in the electric field at lower laser power and saturation at higher laser power. The increase
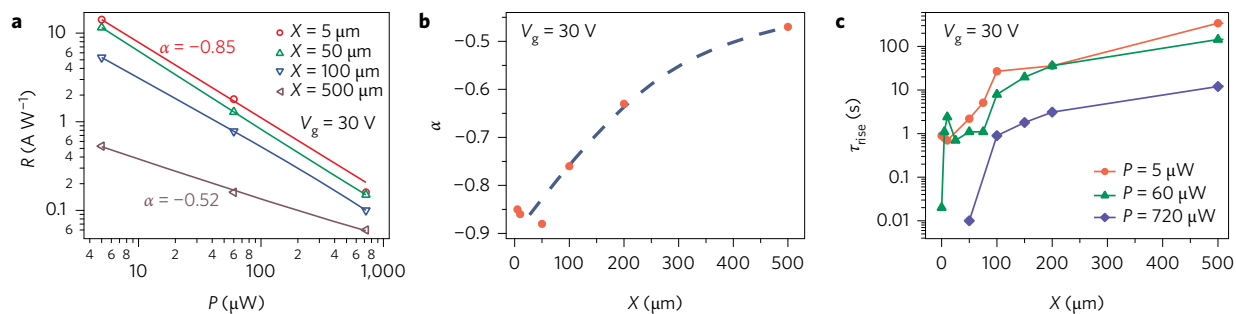
Figure 3 | Laser power-dependent photoresponsivity, and position-sensitive response time. a, Log–log plot of photoresponsivity R as a function of incident laser power P for a few illumination positions on the GFET. Solid lines are power-law fits ($R \propto P^\alpha$) to the experimental data (symbols). **b,** Parameter α, extracted from the fits in **a**, as a function of illumination position. The dashed line is a guide to the eye. **c,** Photocurrent rise time (τ_{rise}, extracted from an exponential fit of the rising edge of the time-dependent I_{photo}; see Supplementary Fig. 9 for an example) as a function of laser illumination position X, showing a dramatic reduction of the response time at shorter distance and saturation behaviour at large distance. The response time increases by at least two orders of magnitude from short (<50 μm) to larger (>500 μm) illumination distances, suggesting that the response time may be related to the transport time of the photogenerated carriers in SiC to underneath the graphene.

in the electric field in the vicinity of graphene results in the modulation of graphene conductivity used to detect the light incident on the GFET. To more quantitatively account for our measured photoresponse, the transport of photoexcited charges must also be considered, as discussed later in section 'Model for nonlocal and position dependent photoresponse'.

Position-sensitive, nonlocal, large-area photoresponse

We measured the $I_{ds} - V_g$ characteristics when focusing the laser spot at different positions X on the SiC substrate away from the graphene. Figure 2a presents the dependence of photocurrent on the gate voltage ($I_{photo} - V_g$) for $P = 5$ μW. The most striking feature observed is that the device shows a photoresponse even when the laser is focused far away from the graphene, on the bare SiC substrate. For laser illumination on the graphene ($X = 0$ μm), the photocurrent shows a strong dependence on V_g. As the laser illumination position is moved away from the graphene, the characteristic $I_{photo} - V_g$ curves alter. The photocurrent for both high positive and negative V_g decreases (Fig. 2a), and V_{Dirac} shifts to lower values with increasing distance (Supplementary Section 5). When $X > 100$ μm, the $I_{photo} - V_g$ characteristics become nearly independent of V_g, and no clear Dirac point is observed, indicating a reduction of the electric field effect at the graphene with increasing distance. This is also seen in transconductance g_m (= dI_{photo}/dV_g) versus distance plots (Supplementary Section 6). These observations clearly indicate that the photoresponse of our device is sensitive to the distance of illumination from the graphene.

The time-dependent photocurrent ($I_{photo} - t$) measurements show a faster photoresponse and a larger steady-state photocurrent (~75 μA) when the illumination ($P = 5$ μW) is centred on the graphene ($X = 0$ μm) (Fig. 2b). With increasing distance, photoresponse is reduced (lower steady-state photocurrent, consistent with the distance-dependent transfer characteristics in Fig. 2a) and is slower compared to illumination on the graphene. Eventually, a much smaller photocurrent (few μA) is observed when the illumination ($P = 5$ μW) position is 500 μm away from the graphene. Interestingly, the same device shows a higher photocurrent (compared to the photocurrent for $P = 5$ μW) even at a distance greater than 1,000 μm when a higher incident laser power ($P = 720$ μW) is used (Fig. 2c; Supplementary Section 7). A photocurrent overshoot[30,31] in the on/off switching is observed for illumination on or near the graphene ($0 \leq X < 10$ μm) with a high laser power (Supplementary Section 7). We found that both the photocurrent and photoresponsivity do not change significantly up to distances of ~100 μm, and then they decrease by more than one order of magnitude with increasing distance (Fig. 2c,d).

This trend suggests that the electric field experienced by the graphene decreases significantly when the illumination position moves far away from the graphene. As shown in Fig. 2d, even where the laser illumination position is 500 μm away from the graphene, our device still exhibits a notable photoresponsivity (~500 mA W^{-1} at $P = 5$ μW and ~60 mA W^{-1} at $P = 720$ μW). This clearly shows that a precise positioning of the laser within the specific area of our device is not required to induce the photoresponse.

The dependence of photoresponsivity on the incident laser power for all illumination positions follows a power law, $R \propto P^\alpha$, where α is in the range of −0.52 to −0.85 (Fig. 3a). A non-unity exponent (deviating from −1) is generally attributed to the presence of defect states[32,33]. Therefore, the observed increase in the exponent α with increasing distance (Fig. 3b) may suggest that when the illumination positions are far away from the graphene, more charge carriers are trapped by defect states. This is also consistent with a longer response time for larger illumination distances (Fig. 3c and Supplementary Section 8), where the photo-generated carriers in SiC travel a longer distance to reach the location under the graphene, resulting in a delay in the occurrence of the field effect in graphene and a longer response time. In addition, for a shorter illumination distance (closer to the graphene and shorter response time), the change in electric field is also higher, which induces a larger number of photo-modulated carriers in the graphene.

Model for nonlocal and position-dependent photoresponse

We have developed a model for the position-dependent photoresponse. The model assumes that the graphene response is determined by the photo-generated charge carriers in the SiC substrate that are transported by the electric field to immediately beneath the graphene. A fraction of transported charge carriers may become trapped during transport at defect and impurity sites, and recombine with their opposite charges, and are thus unable to affect the GFET response. The model considers the graphene photoresponsivity for steady-state laser illumination conditions (equilibrium between photoexcitation and recombination during transport), but does not account for time-dependent transients.

In the model, the electric field is generated by V_g between the graphene and backgate. A two-dimensional map of the electric field within the substrate for $V_g = +30$ V was simulated with COMSOL Multiphysics (Fig. 4a–d)[26]. Electron–hole pairs are produced in SiC along the laser path due to light absorption, and are transported under the influence of the electric field E within the substrate at a velocity

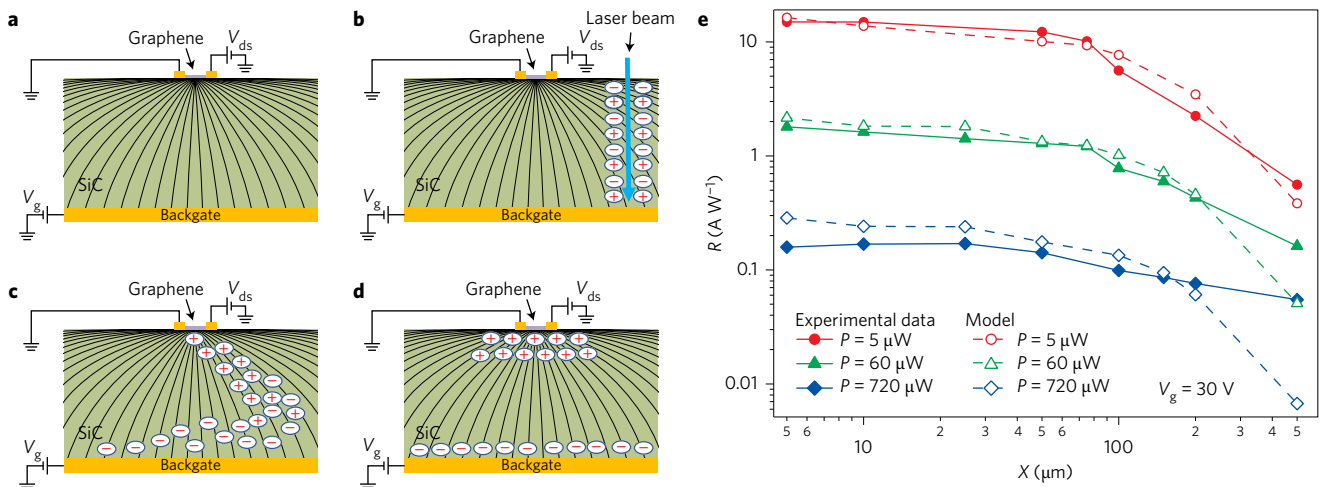$$\mathbf{v}(x, z) = \mu \mathbf{E}(x, z) \tag{1}$$

671

Figure 4 | Model for position-sensitive photoresponse of the GFET. a, Electric field E generated by a gate voltage bias V_g between the graphene and backgate, computed using COMSOL Multiphysics. **b**, Electron–hole pairs are generated along the laser path due to light absorption. The production of electron–hole pairs along the laser path is directly related to the attenuation (absorption) of the 532 nm laser in the SiC substrate. **c**, A balance is reached between the generation and transport of charges and their recombination, which occurs during transport of these charges toward the graphene. **d**, The model assumes that the conductivity change within graphene is related to the charges transported to the closest vicinity to graphene. Remaining electrons and holes eventually recombine with their opposite charge, and the graphene current will return to pre-illumination levels. **e**, The model (dashed line with open symbols) is fitted to experimental photoresponsivity data (solid lines with filled symbols) with the following fitting parameters: recombination length $\varepsilon = 21.2$ μm, normalization constant $\beta = 84.7$ A and nonlinearity of graphene response $\gamma = 0.19$.

where z is the depth into the substrate (with graphene located at $z = 0$) and μ is the charge carrier mobility[34]. At each lateral illumination distance x from the graphene, a series of sample points at a range of depths within the entire substrate are used as starting points for a charge carrier. A sample charge carrier is moved to a new location within a predefined time step t_s:

$$\Delta x_i = t_s v_x(x, z)$$
$$\Delta z_i = t_s v_z(x, z) \tag{2}$$

where i is the iteration number. The total distance travelled, d_{total}, is

$$d_{total} = \sum_1^l \sqrt{\Delta x_i^2 + \Delta z_i^2} \tag{3}$$

where l is the number of iterations, determined by the total number of steps taken (typically several hundred). While undergoing transport in SiC, the electron or hole recombines with its opposite charge within a characteristic distance known as the recombination length, $\varepsilon = 1/\phi\delta$, where ϕ is the recombination cross-section and δ is the density of recombination sites. These recombination sites are considered to be impurities and defects within the SiC substrate. A fraction of charge carriers escape recombination and are transported to the vicinity of the graphene from the illumination position x, with a characteristic transport factor given by

$$T(x) = \exp(-d_{total}/\varepsilon) \tag{4}$$

The number of charges transported to the vicinity of the graphene is the product of the transport factor T and the number of photo-generated charges within the substrate (which is linearly proportional to laser power P). For simplicity, we also assume that without illumination the graphene is relatively undoped (a reasonable approximation for our device). The photocurrent generated (induced change of I_{ds}), I_{photo}, is nonlinearly dependent on the total number of charges that are transported to the vicinity of the graphene:

$$I_{photo}(x, P) = \beta \left[T(x) \frac{P}{P_0} \right]^\gamma \tag{5}$$

where P is the incident laser power, $P_0 = 1$ W is the normalizing power, γ measures the nonlinearity of the graphene response, and β is a normalization constant. With simple modifications (introducing the appropriate sign and offset in the above equation), our model can also be used to treat the case where the unilluminated graphene has some initial doping, as described in Supplementary Section 4. The graphene photocurrent is then converted to photoresponsivity by dividing by P:

$$R_{mod}(x, P) = \frac{\beta}{P} \left[T(x) \frac{P}{P_0} \right]^\gamma \tag{6}$$

The photoresponsivity predicted by the model is calculated by fitting the experimental photoresponsivity data for all laser powers using $\beta = 84.7$ A, $\gamma = 0.19$ and $\varepsilon = 21.2$ μm. This value of the recombination length ε is reasonable when considering the range of values for impurity/defect cross-sections, $\phi = 10^{-18}$ to 10^{-14} cm^2 (refs 35–38), and densities, $\delta = 10^{14}$ to 10^{20} cm^{-3} (refs 39, 40), for SiC. A comparison of the model photoresponsivity against the experimentally measured photoresponsivity for different laser powers is presented in Fig. 4e. We found that our model can explain the nonlocal position-dependent photoresponsivity data measured at 532 nm (Fig. 4e) and other wavelengths (Supplementary Section 4). We note that this model does not adequately describe the behaviour of graphene photoresponsivity at distances greater than 200 μm. This discrepancy (which is greater for higher powers) may be due to the high density of electrons and holes created along the path of the laser beam, which may modify the recombination length near the laser beam path within the SiC. Additionally, the precision of delivery of the illumination to a narrow spot may be compromised due to scattering within the substrate and reflection from the backgate. The light may scatter towards locations closer to the graphene, inducing charge carriers closer to the graphene and generating a response that would otherwise not be expected. With the relatively good fit to our data, the developed model has been shown to be suitable for aiding our understanding of the physical mechanisms of the GFET position-dependent photoresponse. The model can also be applied for a variety of gate voltages, wavelengths

of incident light and GFET dimensions. Because the device response depends on both the position of the illumination and laser intensity, measuring the responses from multiple, spatially separated GFET sensors can facilitate disentangling the effects of illumination position and intensity (Supplementary Sections 10 and 11). If our demonstrated position-dependent photodetectors are implemented into arrays, they may be promising for use in imaging applications such as digital photography.

Conclusions

We have demonstrated that the photoresponse in GFETs allow non-local, position-sensitive and large-area photodetection. The photo-response characteristics of our devices can be controlled by simply varying the illumination distance from the graphene. The device shows substantial photoresponsivity, even when the light is incident as far as 500 μm from the graphene channel for $P = 5$ μW. We expect that our devices will show a photoresponse for even larger distances (centimetre-scale) if the illumination power is increased. In contrast, all the previous graphene photodetectors are based on local detection, where the illumination occurs either on or very close to the graphene. Consequently, they do not exhibit position sensitivity over such a large detection area. We have developed a numerical model that explains the field-effect photodetection mechanism and the experimental observation of position-dependent photocurrent characteristics for our devices. The relatively simple and unique device configuration (a combination of small graphene and large SiC substrate) results in both the position sensitivity and large photodetection area. In addition, the moderately high photo-responsivity of our devices (higher than standard graphene photo-detectors, but lower than some graphene–nanomaterial hybrid detectors[2,8,9,13,14]) meets the photoresponsivity required for most practical applications (~1 A W^{-1}) (ref. 7). We also anticipate that the photoresponsivity can be further improved by optimizing the fabrication processes and measurement conditions (for example, increasing the source–drain bias voltage, reducing the laser power, and so on). Another interesting aspect of our results is that the photo-activated field-effect mechansim enables a backgated field-effect transistor (FET) with graphene on insulating SiC substrates, which would not exhibit an observable field effect without illumination. This approach can be generalized to fabricate FETs using other two-dimensional materials on other insulating/wide-bandgap semiconductor substrates, without the need to fabricate multilayer structures for top gates. The use of a wide range of undoped semiconductor substrates, differing in bandgaps and other electro-optical properties, will allow the detection of light over a wide range of wavelengths (Supplementary Section 12). This flexibility will be valuable when employing such GFET-based photodetectors in future nanoelectronics and optoelectronics.

Methods

Methods and any associated references are available in the online version of the paper.

References

1. Withers, F., Bointon, T. H., Craciun, M. F. & Russo, S. All-graphene photodetectors. *ACS Nano* **7**, 5052–5057 (2013).
2. Freitag, M., Low, T., Xia, F. N. & Avouris, P. Photoconductivity of biased graphene. *Nat. Photon.* **7**, 53–59 (2013).
3. Xia, F. *et al.* Photocurrent imaging and efficient photon detection in a graphene transistor. *Nano Lett.* **9**, 1039–1044 (2009).
4. An, X., Liu, F., Jung, Y. J. & Kar, S. Tunable graphene–silicon heterojunctions for ultrasensitive photodetection. *Nano Lett.* **13**, 909–916 (2013).
5. Liu, N. *et al.* Large-area, transparent, and flexible infrared photodetector fabricated using p–n junctions formed by n-doping chemical vapor deposition grown graphene. *Nano Lett.* **14**, 3702–3708 (2014).
6. Shi, Y., Fang, W., Zhang, K., Zhang, W. & Li, L. J. Photoelectrical response in single-layer graphene transistors. *Small* **5**, 2005–2011 (2009).
7. Liu, C.-H., Chang, Y.-C., Norris, T. B. & Zhong, Z. Graphene photodetectors with ultra-broadband and high responsivity at room temperature. *Nat. Nanotech.* **9**, 273–278 (2014).
8. Mueller, T., Xia, F. N. A. & Avouris, P. Graphene photodetectors for high-speed optical communications. *Nat. Photon.* **4**, 297–301 (2010).
9. Xia, F. N., Mueller, T., Lin, Y. M., Valdes-Garcia, A. & Avouris, P. Ultrafast graphene photodetector. *Nat. Nanotech.* **4**, 839–843 (2009).
10. Vicarelli, L. *et al.* Graphene field-effect transistors as room-temperature terahertz detectors. *Nat. Mater.* **11**, 865–871 (2012).
11. Pospischil, A. *et al.* CMOS-compatible graphene photodetector covering all optical communication bands. *Nat. Photon.* **7**, 892–896 (2013).
12. Gan, X. *et al.* Chip-integrated ultrafast graphene photodetector with high responsivity. *Nat. Photon.* **7**, 883–887 (2013).
13. Konstantatos, G. *et al.* Hybrid graphene–quantum dot phototransistors with ultrahigh gain. *Nat. Nanotech.* **7**, 363–368 (2012).
14. Roy, K. *et al.* Graphene–MoS$_2$ hybrid structures for multifunctional photoresponsive memory devices. *Nat. Nanotech.* **8**, 826–830 (2013).
15. Zhang, B. Y. *et al.* Broadband high photoresponse from pure monolayer graphene photodetector. *Nat. Commun.* **4**, 1811 (2013).
16. Huang, Y. Q., Zhu, R. J., Kang, N., Du, J. & Xu, H. Q. Photoelectrical response of hybrid graphene–PbS quantum dot devices. *Appl. Phys. Lett.* **103**, 143119 (2013).
17. Li, J., Niu, L., Zheng, Z. & Yan, F. Photosensitive graphene transistors. *Adv. Mater.* **26**, 5239–5273 (2014).
18. Sun, Z. & Chang, H. Graphene and graphene-like two-dimensional materials in photodetection: mechanisms and methodology. *ACS Nano* **8**, 4133–4156 (2014).
19. Gabor, N. M. *et al.* Hot carrier-assisted intrinsic photoresponse in graphene. *Science* **334**, 648–652 (2011).
20. Xu, X., Gabor, N. M., Alden, J. S., van der Zande, A. M. & McEuen, P. L. Photo-thermoelectric effect at a graphene interface junction. *Nano Lett.* **10**, 562–566 (2010).
21. Echtermeyer, T. J. *et al.* Photothermoelectric and photoelectric contributions to light detection in metal–graphene–metal photodetectors. *Nano Lett.* **14**, 3733–3742 (2014).
22. Kim, M. H. *et al.* Photothermal response in dual-gated bilayer graphene. *Phys. Rev. Lett.* **110**, 247402 (2013).
23. Peters, E. C., Lee, E. J. H., Burghard, M. & Kern, K. Gate dependent photocurrents at a graphene p–n junction. *Appl. Phys. Lett.* **97**, 193102 (2010).
24. Kildemo, M. Optical properties of silicon carbide polytypes below and around bandgap. *Thin Solid Films* **455–456**, 187–195 (2004).
25. Limpijumnong, S., Lambrecht, W. R. L., Rashkeev, S. N. & Segall, B. Optical-absorption bands in the 1–3 eV range in n-type SiC polytypes. *Phys. Rev. B* **59**, 12890–12899 (1999).
26. Foxe, M. *et al.* Graphene field-effect transistors on undoped semiconductor substrates for radiation detection. *IEEE Trans. Nanotechnol.* **11**, 581–587 (2012).
27. Cazalas, E. *et al.* Hysteretic response of chemical vapor deposition graphene field effect transistors on SiC substrates. *Appl. Phys. Lett.* **103**, 053123 (2013).
28. Da Silva, C. R. S., Justo, J. F. & Pereyra, I. Crystalline silicon oxycarbide: is there a native oxide for silicon carbide? *Appl. Phys. Lett.* **84**, 4845–4847 (2004).
29. Amy, F., Soukiassian, P., Hwu, Y. & Brylinski, C. Si-rich 6H- and 4H-SiC(0001) 3×3 surface oxidation and initial SiO$_2$/SiC interface formation from 25 to 650 °C. *Phys. Rev. B* **65**, 165323 (2002).
30. Letov, V. *et al.* Transient photocurrent overshoot in quantum-well infrared photodetectors. *Appl. Phys. Lett.* **79**, 2094–2096 (2001).
31. Letov, V. *et al.* Experimental observation of transient photocurrent overshoot in quantum well infrared photodetectors. *Infrared Phys. Technol.* **42**, 243–247 (2001).
32. Xu, H. *et al.* High responsivity and gate tunable graphene–MoS$_2$ hybrid phototransistor. *Small* **10**, 2300–2306 (2014).
33. Buscema, M. *et al.* Fast and broadband photoresponse of few-layer black phosphorus field-effect transistors. *Nano Lett.* **14**, 3347–3352 (2014).
34. Marinella, M. J. *et al.* Carrier generation lifetimes in 4H-SiC MOS capacitors. *IEEE Trans. Electron Dev.* **57**, 1910–1923 (2010).
35. Hemmingsson, C., Son, N. T., Kordina, O., Janzén, E. & Lindström, J. L. Capture cross sections of electron irradiation induced defects in 6H–SiC. *J. Appl. Phys.* **84**, 704–708 (1998).
36. Gong, M., Fung, S., Beling, C. D. & You, Z. Electron-irradiation-induced deep levels in n-type 6H–SiC. *J. Appl. Phys.* **85**, 7604–7608 (1999).
37. David, M. L. *et al.* Electrically active defects in irradiated 4H–SiC. *J. Appl. Phys.* **95**, 4728–4733 (2004).

38. Klein, P. B. *et al.* Lifetime-limiting defects in n⁻ 4H–SiC epilayers. *Appl. Phys. Lett.* **88**, 052110 (2006).
39. Glaser, E. *et al.* Infrared PL signatures of n-type bulk SiC substrates with nitrogen impurity concentration between 10^{16} and 10^{17} cm^{-3}. *Mater. Sci. Forum* **600–603,** 449–452 (2009).
40. Matsumoto, T., Nishizawa, S. & Yamasaki, S. Calculation of lattice constant of 4H–SiC as a function of impurity concentration. *Mater. Sci. Forum* **645–648,** 247–250 (2010).

Author contributions

B.K.S., T.-F.C. and I.C. fabricated the devices. B.K.S. and T.-F.C. carried out the measurements. B.K.S. analysed the data. Y.P.C. supervised the project. E.C. and I.J. developed the model with input from the other authors. All authors contributed to interpretation of the results and writing of the manuscript.

Additional information

Supplementary information is available in the online version of the paper. Reprints and permissions information is available online at www.nature.com/reprints. Publisher's note: Springer Nature remains neutral with regard to jurisdictional claims in published maps and institutional affiliations. Correspondence and requests for materials should be addressed to Y.P.C.

Competing financial interests

The authors declare no competing financial interests.

Methods

Device fabrication. Single-layer graphene was prepared by micromechanical exfoliation from highly ordered pyrolytic graphite (HOPG). The graphene was transferred onto a 6H-SiC substrate (PAM-Xiamen, resistivity $\geq 1 \times 10^5$ Ω cm) with a thickness of 416 μm by a polymer assisted transfer method[41]. The source and drain electrical contacts to the graphene were fabricated using electron-beam lithography followed by deposition of 5 nm Cr and 65 nm Au. The channel defined by the electrodes was ~2 μm long and ~4 μm wide. Finally, the Cr (5 nm)/Au (65 nm) was also deposited on the back side of the SiC to make the backgate contact.

Device characterization. The Raman spectra of graphene on the SiC substrate were measured using a Horiba Jobin Yvon Xplora confocal Raman microscope. After fabricating the devices, we performed their initial electrical testing. The devices were then wire-bonded to chip carriers and placed in a chip socket in a motorized sample stage (Marzhauser Wetzlar) for the position-dependent photoresponse measurements. Computer-guided micropositioning of the sample was used to change the location of illumination positions across the device. A laser beam with a wavelength of 532 nm was focused through ×100 objective lens (NA = 0.6) onto the device. The size of laser beam incident on the device was ~0.6 μm. The incident laser power was calibrated using a power meter. Nonlocal photoresponse measurements were also performed using other illumination laser wavelengths (Supplementary Section 4). For each illumination position, the two-terminal d.c. electronic and optoelectronic characterization of the device was performed using two Keithley 2400 source meters.

Data availability. The data that support the plots within this paper and other findings of this study are available from the corresponding author upon reasonable request.

References

41. Dean, C. R. *et al.* Boron nitride substrates for high-quality graphene electronics. *Nat. Nanotech.* **5,** 722–726 (2010).